PCCP

PAPER

View Article Online
View Journal | View Issue

Cite this: *Phys. Chem. Chem. Phys.*, 2025, **27**, 4627

Magnetic quantum phase transition extension in strained P-doped graphene

Natalia Cortés, *[a] J. Hernández-Tecorralco,[b] L. Meza-Montes,[c] R. de Coss[de] and Patricio Vargas[f]

Received 3rd December 2024,
Accepted 21st January 2025

DOI: 10.1039/d4cp04573d

rsc.li/pccp

We explore quantum-thermodynamic effects in a phosphorous (P)-doped graphene monolayer subjected to biaxial tensile strain. Introducing substitutional P atoms in the graphene lattice generates a tunable spin magnetic moment controlled by the strain control parameter ε. This leads to a magnetic quantum phase transition (MQPT) at zero temperature modulated by ε. The system transitions from a magnetic phase, characterized by an out-of-plane sp^3 type hybridization of the P–carbon (P–C) bonds, to a non-magnetic phase when these bonds switch to in-plane sp^2 hybridization. Employing a Fermi–Dirac statistical model, we calculate key thermodynamic quantities such as the electronic entropy S_e and electronic specific heat C_e. At finite temperatures, we find a MQPT extension characterized by S_e and C_e, where both display a distinctive Λ-shape profile as a function of ε. These thermodynamic quantities sharply increase up to ε = 5% in the magnetic regime, followed by a sudden drop at ε = 5.5%, transitioning to a linear dependence on ε in the nonmagnetic regime. This controllable magnetic-to-nonmagnetic switch offers potential applications in electronic nanodevices operating at finite temperatures.

I. Introduction

The transformation of one state of matter into another one driven by temperature T is typically characterized by a phase transition, where both states of matter (or phases) are separated by a boundary and touching at a critical T value. When a phase transition occurs in a magnetic material, the magnetic moment of the electrons plays the major role as T varies, *i.e.*, the orientation of the electron spins changes due to thermal fluctuations induced by T. Depending on the magnetic properties of the material (iron, for example), one can observe a magnetic phase transition as a function of temperature, going from a magnetic state into a nonmagnetic state at a critical T value.[1]

At the quantum level, the nature of phase transitions can be different as they manifest in a quantum critical region, where quantum and thermal fluctuations are equally important.[2] This type of phase transition starts at absolute zero (T = 0 K) and can continue as T increases to some small finite value, as seen in a ferromagnetic phase diagram controlled by an applied magnetic field, for example.[2] At T = 0 the state is denominated quantum phase transition (QPT),[2] and the main feature of a QPT is the so-called quantum critical point (QCP), where thermal fluctuations are suppressed and quantum fluctuations are predominant in the system. The quantum fluctuations are driven by a nonthermal control parameter such as an applied magnetic field, the amount of charge carriers, pressure, or strain, among others.[2,3]

Graphene is a versatile material where magnetic, topological, or quantum phase transitions can appear, which are ruled by diverse control parameters.[4–7] Pristine graphene is a nonmagnetic material, and some ways to induce magnetism in it are through defects,[8] creating samples with defined edges,[9] or by adding foreign atoms to their lattice.[10] It has been shown that phosphorous (P) atoms are good candidates to produce magnetism in graphene by substitutional doping.[11,12] Graphene also allows the application of strain at finite temperatures, where its two-dimensional (2D) hexagonal structure possesses exceptional mechanical properties, allowing large deformations without breaking.[13] Uniaxial and biaxial strain are experimentally accessible techniques that can be applied to graphene systems by lattice deformations of its carbon (C) atoms. Strain can be useful as a tool for tuning graphene electronic properties[14] and organic hexagonal shaped 2D systems.[15] Strain can also serve as a way to assist self-assembly of adsorbed atoms on the graphene lattice,[16] and can induce a QPT in magic-angle twisted bilayer graphene.[5]

[a] *Instituto de Alta Investigación, Universidad de Tarapacá, Casilla 7D, Arica, Chile. E-mail: natalia.cortesm@usm.cl*
[b] *Instituto de Física, Universidad Nacional Autónoma de México, Apartado Postal 20-364, Ciudad de México, C.P. 01000, Mexico*
[c] *Instituto de Física, Benemérita Universidad Autónoma de Puebla, Apartado Postal J-48, 72570, Puebla, Mexico*
[d] *Departamento de Física Aplicada, Centro de Investigación y de Estudios Avanzados del IPN, Apartado Postal 73, Cordemex, 97310, Mérida, Yucatán, Mexico*
[e] *Centro Mesoamericano de Física Teórica, Universidad Autónoma de Chiapas, 29050 Chiapas, Mexico*
[f] *Departamento de Física, Universidad Técnica Federico Santa María, 2390123 Valparaíso, Chile*

Density functional theory (DFT) studies show that at $T = 0$ K, a P-impurity atom opens a gap in bulk graphene and induces a narrow band at the Fermi level (E_F), generating magnetism through a large spin-polarized state with spin splitting of 267 meV.[17] This magnetic state is associated with P–C out-of-plane bonds showing sp^3-like hybridization in graphene real-space lattice. As tensile strain is applied on P-doped graphene, the sp^3 electronic configuration remains up to a certain critical strain value, then the hybridization for the atoms changes to sp^2 as strain increases, recovering the flat hexagonal lattice with combined P–C bonds in the constructed supercell. In this process, a magnetic quantum phase transition (MQPT) occurs from a magnetic state to a nonmagnetic state driven by the strain control parameter ε.[17]

One fundamental question may emerge from the above-mentioned processes: what will happen with the predicted MQPT in P-doped graphene when temperature is turned on? To answer this question, we should know how the entropy can influence the MQPT at T above zero. We can access this thermodynamic quantity for electrons through the electronic entropy S_e, and then obtain the electronic specific heat C_e, both by employing Fermi–Dirac statistics. These two thermodynamic–electronic quantities are directly linked to each other by temperature, so they only play a role at finite T. Experimental measurements of S_e have allowed the acquisition of fundamental information about the accessible electronic states of different systems, such as quantum dots[18] and magic angle twisted bilayer graphene.[19,20] It was found that in graphene, doping can induce changes in C_e as a function of T,[21] and edge states in zigzag graphene nanoribbons can improve C_e at low T.[22] Only just a few years ago, it was possible to measure C_e in graphene monolayer by using ultrasensitive calorimetric techniques.[23]

In this work, we theoretically predict both thermodynamic quantities S_e and C_e for strained P-doped graphene at finite temperatures. We find that S_e and C_e are three orders of magnitude larger than strained pristine graphene. We show S_e and C_e are the extensions of the MQPT at finite temperatures with a Λ-type line shape as a function of ε. We can observe the two characteristic magnetic ($0\% \leq \varepsilon \leq 5\%$), and nonmagnetic ($5.5\% \leq \varepsilon \leq 10\%$) regimes are still present in the phase diagram at finite T as compared to $T = 0$ phase diagram. We evaluate three different orders of magnitude for T and find that the Λ-type line shape is preserved. Interestingly, thermal fluctuations present in S_e and C_e do not destroy the quantum critical region found at $T = 0$ phase diagram, instead it is preserved within the same ε values for S_e and C_e at finite T.

II. DFT-thermodynamic model

To obtain the electronic and magnetic properties of strained pristine graphene and strained P-doped graphene (the latter labeled as P-graphene), we performed DFT calculations using a plane-wave and pseudopotential method, as implemented in the QUANTUM-ESPRESSO code.[24,25] Valence electrons were represented by plane waves with a kinetic energy cutoff of 55 Ry (320 Ry for the charge density), while core electrons were replaced by ultrasoft pseudopotentials.[26] We employ the generalized gradient approximation with Perdew–Burke–Ernzerhof (PBE) parametrization[27] for the exchange–correlation functional. A vacuum spacing of 15 Å was used to avoid interaction between periodic images along the z-direction. For all cases, atomic positions were relaxed until the internal forces were below 0.01 eV Å^{-1}. Brillouin zone integrations were carried out with a 21×21 k-point grid[28] using a Methfessel–Paxton scheme smearing[29] with a width of 0.005 Ry for the constructed unit cells for strained pristine graphene and strained P-graphene.

We simulated P substitutional impurities by replacing one C atom from a graphene layer considering a 5×5 graphene supercell. Our model consists of 49 C atoms and one P atom, corresponding to 2.0% of impurities concentration of P atoms.[17] Biaxial tensile strain modulated by the control parameter ε is applied on the systems by increasing the lattice constant as $a = (1 + \varepsilon)a_0$, where a_0 is the unstrained graphene lattice constant, and ε takes values from 0% to 10% because the MQPT extension occurs around the middle of these strain values, as we will see below. Within these DFT calculations at zero temperature, the electronic density of states (DOS) is obtained for strained pristine graphene and strained P-graphene. The DOS, D, we use throughout the paper is the sum of spin up (↑) and spin down (↓), majority and minority components respectively, $D(E, \varepsilon) = D_\uparrow + D_\downarrow$. The density of states depends on both the electronic state with energy eigenvalue E, and the control parameter ε applied on either strained graphene system.

Fig. 1 shows the DOS for strained pristine graphene with ε ranging from 0% to 7%. At zero energy [charge neutrality point (CNP)], $D = 0$ for each ε value, then D linearly increases with different slopes around CNP [up to $D \approx 0.1$ states (eV cell)$^{-1}$].

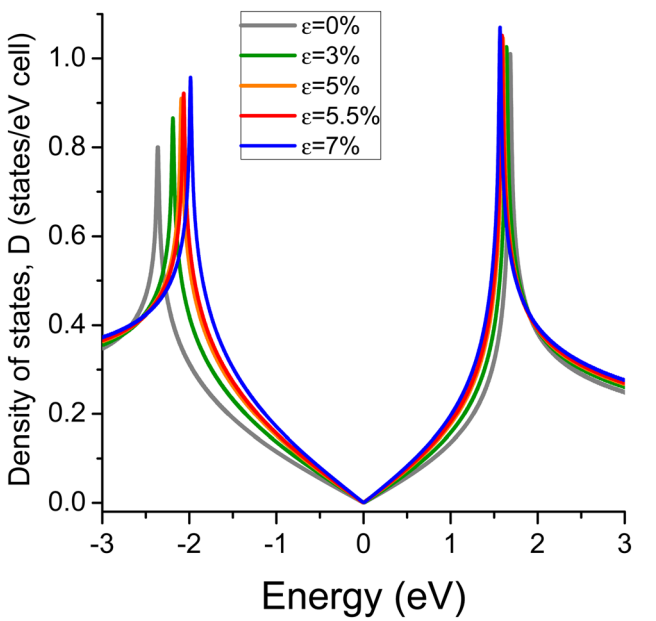

Fig. 1 DOS for strained pristine graphene where $\varepsilon = 0$ represents the unstrained graphene monolayer. The unit cell for pristine graphene has two C atoms. All Fermi levels are set to zero energy.

The two van Hove singularities around CNP are nonsymmetric as we use more than one single orbital for C atoms in our DFT calculations.

When a substitutional P impurity atom is added to the monolayer graphene, the behavior of the DOS drastically changes. In Fig. 2, we show D for strained P-graphene, including contributions of $D_\uparrow$ and $D_\downarrow$ with red and blue lines, respectively. At ε = 0% (top panel), two large spin-splitting peaks appear around E_F (within the energy range $-0.5 \leq E \leq 0.5$ eV). Each peak corresponding to one type of spin density has contributions of the P-impurity and C atoms of graphene, generating a maximum spin magnetic moment (M_S).[30] As strain increases, the spin splitting between both spin densities reduces until they become identical at a critical value $\varepsilon = 5.5\%$, indicating the change from a magnetic ($D_\uparrow \neq D_\downarrow$) to a nonmagnetic state ($D_\uparrow = D_\downarrow$). When $\varepsilon \geq 5.5\%$, the C atoms of the graphene monolayer make room for the P impurity in the hexagonal plane, and the two peaks vanish and merge in the DOS. These latter types of DOS are responsible for the nonmagnetic regime. These changes in the DOS as ε increases are in connection with structural changes in the atomic lattice, as seen in the atomic arrangements shown above the DOS for ε = 0, 5, and 5.5% in Fig. 2. We will discuss these transitions in the next sections.

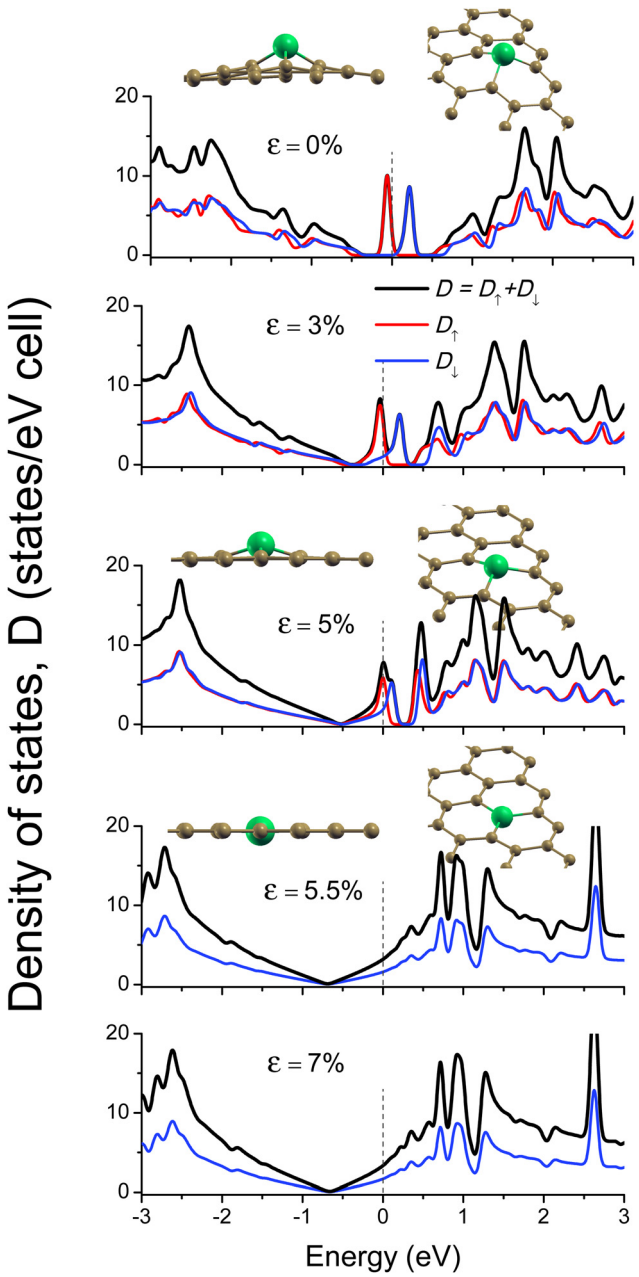

Fig. 2 DOS for strained P-doped graphene. The unit cell for strained P-graphene has 49 C atoms and 1 P atom. The red color lines represent the majority, and blue color lines represent minority spin contributions in all cases. All Fermi levels are set to zero energy. Atomic structures for strain ε = 0, 5, and 5.5% are shown above the corresponding DOS with a side view at the left side and a perspective view on the right side. The small brown spheres represent C atoms, and the large light green sphere the P atom. Notice these images are zoomed areas of the unit cell near the P atom.

We anticipate these previous DOS calculations at T = 0 K do not significantly vary for moderate temperatures, as seen for example in strained organic 2D materials.[15] Under this assumption, we can obtain S_e and C_e at finite T through Fermi–Dirac statistics using the DOS at T = 0 K in the following way. From the constructed graphene supercell, we have that the total number of electrons is N = 201, in which N must be preserved for each system regardless of the T value. First, we can obtain the chemical potential $\mu(T)$ as a function of T for each ε value by inversion of

$$N = 201 = \int_{E_l}^{E_h} D(E,\varepsilon) n_F(E,T,\mu) \mathrm{d}E, \quad (1)$$

where $E_{l(h)}$ is the lowest (highest) electronic energy eigenvalue of the considered graphene system, $n_F(E, T, \mu) = 1/[e^{\beta(E-\mu(T))} + 1]$ is the Fermi–Dirac function distribution with $\beta = 1/k_B T$, and k_B is the Boltzmann constant. All the electronic DOS presented in Fig. 1 and 2 can be used to obtain S_e and C_e at finite temperature $T > 0$. We calculate S_e as

$$S_e(\varepsilon, T) = k_B \int_{E_l}^{E_h} D(E,\varepsilon) \mathcal{F}(n_F) \mathrm{d}E, \quad (2)$$

where

$$\mathcal{F}(E,T,\mu) = -[n_F \ln n_F + (1-n_F)\ln(1-n_F)], \quad (3)$$

is approximated by a Lorentzian-like function

$$L(E,T,\mu) = \frac{1.4}{e^{(|E-\mu(T)|/2k_B T)^{3/2}} + 1}, \quad (4)$$

where its width is T dependent with full width at half maximum (FWHM) of $\simeq 4k_B T$. By considering low and high T, we obtain excellent agreement between eqn (3) and (4) as $\mathcal{F}(E, T, \mu) \cong L(E, T, \mu)$, see Fig. 3. Hence, we can use the L function in eqn (4), which plays the role of a filter around E_F for each DOS, as it captures states of the DOS of width $\simeq 4k_B T$. This approximation can be applied to other 2D materials because L is a generic function depending on the system's energy

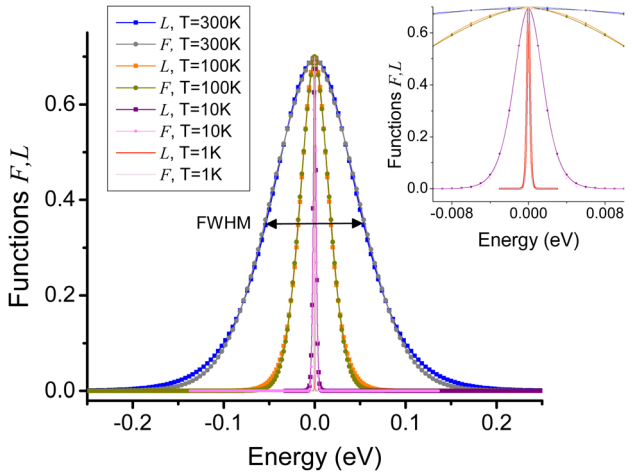

Fig. 3 Comparison plot between $\mathcal{F}$ function in eqn (3) and L function in eqn (4) at $\mu = 0$ and different temperatures as indicated. The black horizontal arrow indicates the full width at half maximum for the curves at $T = 300$ K, and the right inset presents a zoom area near zero energy, showing high agreement for both functions at all T we consider.

eigenvalues E, μ and T, as demonstrated for different quantum structures.[31,32] Therefore, eqn (2) transforms as

$$S_e(\varepsilon, T) \cong k_B \int_{E_l}^{E_h} D(E, \varepsilon) L(E, T, \mu) dE. \quad (5)$$

Through eqn (5), we calculate the electronic specific heat C_e as

$$C_e(\varepsilon, T) = T \frac{dS_e}{dT}. \quad (6)$$

Eqn (5) and (6) can be resolved either as a function of ε or T. When as a function of ε, we will get information about the accessible electronic states and the MQPT extension with a Λ-type profile for P-graphene at different temperatures.

III. Finite-temperature results

Fig. 4 shows S_e in left panels, and C_e in right panels for strained pristine graphene (top panels) and strained P-graphene (bottom panels). We emphasize that the thermodynamic quantities are calculated per unit cell in each case.[33] When pristine graphene is biaxially strained, S_e and C_e show similar behavior as seen in panels (a) and (b). Both quantities monotonically increase as T increases, but C_e increases faster than S_e, and their lowest values occur for the unstrained case $\varepsilon = 0$, while the maxima are for $\varepsilon = 7\%$. The inset in Fig. 4(a) shows that S_e is a linear function of T up to $T \simeq 20$ K, and C_e is linear with T up to $T \simeq 8$ K as shown in the inset of Fig. 4(b). These monotonically thermodynamic responses for strained pristine graphene do not show significant variations as ε changes and T increases.

However, S_e and C_e substantially change their behavior for strained P-graphene, as shown in Fig. 4(c) and (d), respectively. Both quantities are three orders of magnitude larger than for strained pristine graphene due to the contribution of the P-impurity atom states. For P-graphene, the L function in eqn (4) captures more available states of each DOS as T increases, as one can infer from Fig. 2 in connection with Fig. 3. These captured states are mainly due to the spin-polarized peaks around E_F for each strain value. The highest S_e and C_e magnitudes occur for $\varepsilon = 5\%$ instead of $\varepsilon = 7\%$ as in the pristine case. For $\varepsilon = 5\%$, the L function captures a maximum around E_F, see the mid panel in Fig. 2, indicating the highest quantity of available electronic states occur at $\varepsilon = 5\%$. When $\varepsilon > 5\%$, S_e and C_e linearly increase as T increases. For these strain values ($\varepsilon > 5\%$), one can see from the DOS in Fig. 2 that the peak states are no longer distinguishable near E_F, therefore the L function captures less available states and S_e and C_e are lower than for $\varepsilon = 5\%$. At $T \leq 20$ K, S_e and C_e show high similarity, linearly increasing with T as shown in insets of Fig. 4(c) and (d). The non monotonically behavior for S_e and C_e as a function of T, and the sudden jump at $\varepsilon = 5\%$ for all T, indicates that a phase transition can be taking place in strained P-graphene at finite T.

To get insight into that peculiar behavior for strained P-graphene, we present in Fig. 5, S_e in panel (a), and C_e in panel (b), both as a function of ε and three different T values, $T = 1$ K, $T = 10$ K and $T = 100$ K. We choose the curve for $T = 100$ K [red triangles in panel (a) and red asterisk symbols in panel (b)] for the following description; however, the same applies as T decreases up to $T = 1$ K (with the exception of their numerical magnitudes). We also include results for the spin magnetic moment, M_S, in panel (c), to highlight the MQPT at $T = 0$ K. All these results are particularly interesting due to several factors.

At finite temperatures, both S_e and C_e exhibit a strikingly similar behavior. Their respective line shapes increase sharply with rising ε, reaching a peak value of ≈ 0.2 eV K^{-1} at $\varepsilon = 5\%$. Beyond this point, both quantities suddenly drop at $\varepsilon = 5.5\%$, with a magnitude of ≈ 0.1 eV K^{-1}. For $\varepsilon \geq 5.5\%$, S_e and C_e gradually increase with ε, displaying minor variations in their linear profiles as T rises. This overall behavior, characterized by a Λ-type line shape that remains largely consistent with changing T,[34] suggests the presence of two distinct regimes when in comparison to the MQPT observed at $T = 0$, as depicted in Fig. 5, panel (c).

In Fig. 5(c), we show the MQPT with M_S as a function of ε at $T = 0$,[17] where we can identify two regimes, the first one is the magnetic phase, in the range $0\% \leq \varepsilon \leq 5.5\%$ (violet color area). In the second regime in the range $5.5\% \leq \varepsilon \leq 10\%$ (green color area), a nonmagnetic phase ($M_S = 0$) is seen. This MQPT is closely related to the electronic configuration of the electron states that contribute to S_e and C_e. When $\varepsilon < 5.5\%$, the substitutional P impurity atom is positioned above the graphene plane because the P atom does not fit into the graphene hexagonal lattice. However, when $\varepsilon \geq 5.5\%$, the P impurity aligns within the same plane as graphene, transitioning from an sp^3-like to an sp^2 electronic configuration, see atomic structures in Fig. 2. This transition causes the spin-polarized state for the P atom to go to zero ($M_S = 0$) as $\varepsilon \geq 5.5\%$, leading the system from a magnetic phase into a nonmagnetic one, and the MQPT is manifested in strained P-graphene at $T = 0$.

As Fig. 5 panels (a) and (b) show, S_e and C_e increase for the same strain values when the magnetism goes down at $T = 0$, see violet regions in all panels of Fig. 5. In this regime, the strained P-graphene system increases the quantity of available electronic

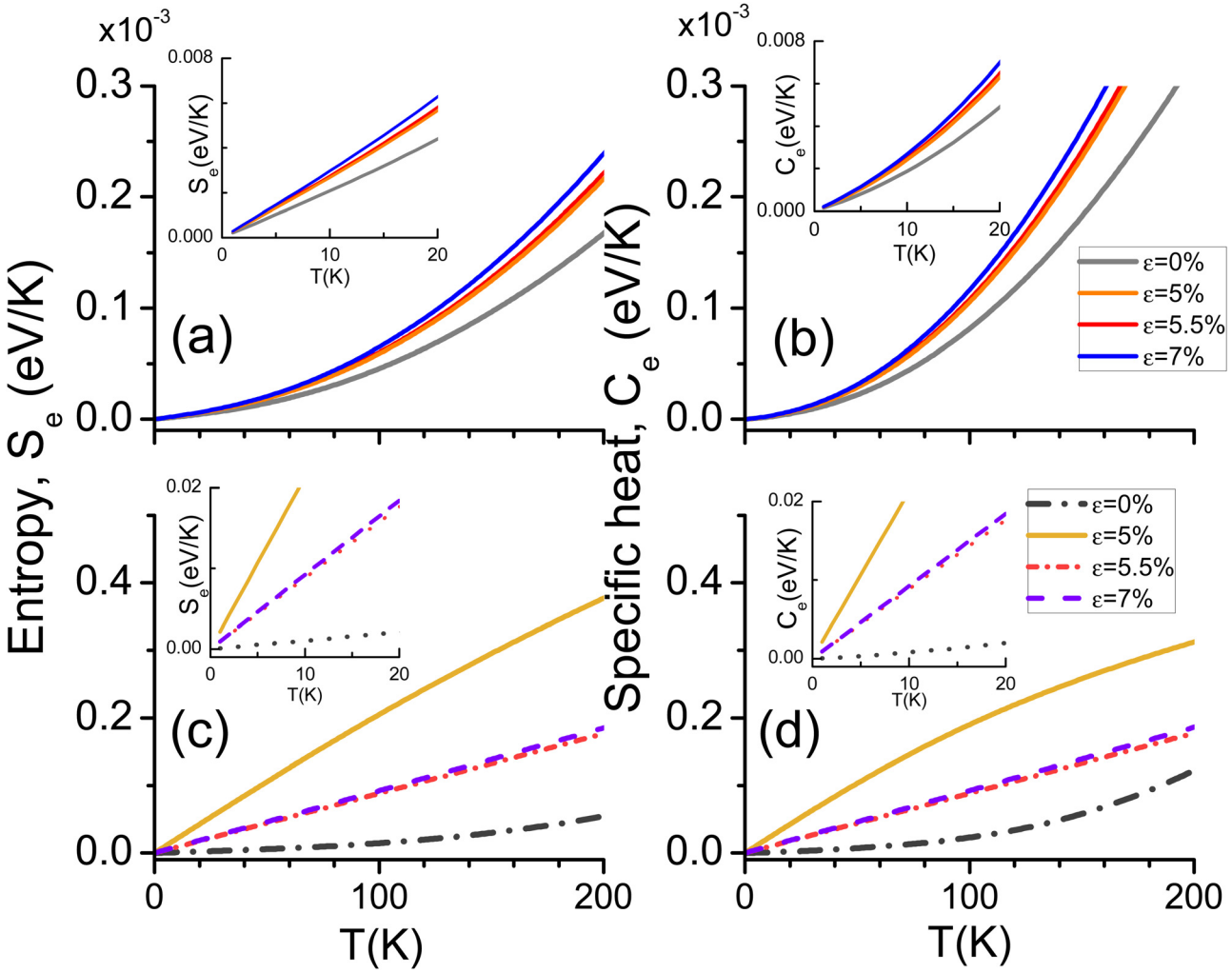

Fig. 4 (a) and (c) Electronic entropy (S_e) calculated through eqn (5); (b) and (d) electronic specific heat (C_e) from eqn (6), both per supercell. All quantities as a function of temperature T for different values of ε as indicated. Top panels (a) and (b): Strained pristine graphene, bottom panels (c) and (d): strained P-doped graphene. Insets show a zoom for each quantity with T going from 1 K to 20 K. Vertical scales in (a) and (b) and their respective insets times 10^{-3}. Notice ε = 0% corresponds to unstrained graphene in each plot.

states as long as the P-atom induces magnetism up to ε = 5%. Then S_e and C_e abruptly drop at ε = 5.5%. Since S_e and C_e involve electronic states within a small energy range of width $\simeq 4k_BT$, and very close to E_F, the phenomenon of the transition between ε = 5% and ε = 5.5% is evident in the DOS shown in Fig. 2. The DOS around E_F for ε = 5% is completely different compared to the DOS for ε = 5.5%. The first one shows a peak, and the latter a small curvature around E_F; the DOS significantly decreases between these two strain values. This explains the abrupt drop for S_e and C_e at ε = 5.5%.

Following the drop of S_e and C_e (green zone in panels (a) and (b) of Fig. 5), both thermodynamic quantities show a linear behavior as ε increases, with no significant changes in their line profiles for the three different temperatures. Is in this regime where the magnetism vanishes as compared to the MQPT in panel (c). The MQPT extension is then observed as the Λ-type line profile in S_e and C_e as a function of ε and T different from zero.

Notably, S_e and C_e reveal a critical region for ε in the range 5% $\leq \varepsilon \leq$ 5.5% (see shading gray rectangle in each plot), just when the system transitions from a magnetic phase to a nonmagnetic one (or *vice versa*) even at temperatures higher than zero. This critical region can tell us that there is a mixing of quantum and thermal fluctuations competing to lower the electronic entropy and specific heat to reach a stable state for the system. In other words, the thermodynamic quantities S_e and C_e for $T \neq 0$ may indicate quantum criticality within this region.[2] We highlight that the thermodynamic quantities reported here are for temperatures up to T = 200 K. Although extending the analysis to higher temperatures is feasible, our focus is based on electronic specific heat experiments,[23] which are done within this T range, capturing the behavior for moderate temperatures.

IV. Conclusions

Strained phosphorous-doped graphene exhibits emergent magnetism as long as a sp^3-like hybridization of the P–C bonds takes place in the system. The applied strain control parameter ε, plays a critical role in modulating the sp^3-like electronic

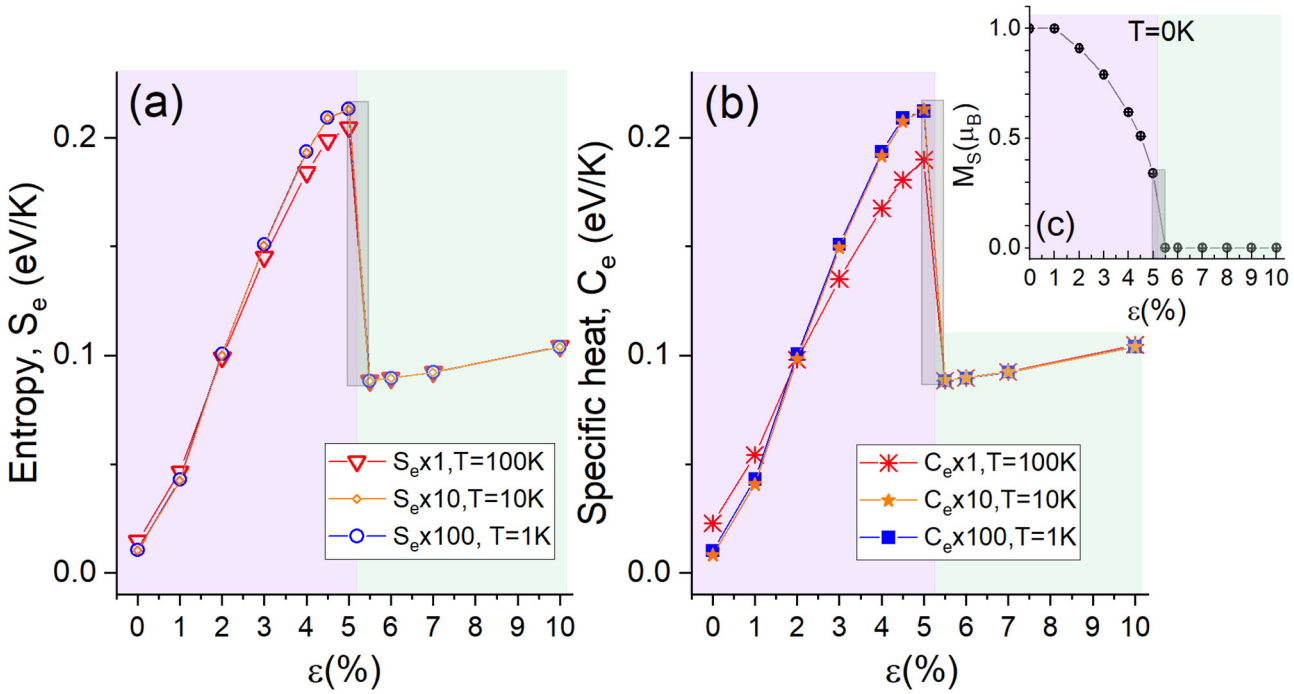

Fig. 5 (a) Electronic entropy S_e, (b) electronic specific heat C_e, (c) spin magnetic moment (M_S) at T = 0 K. All quantities calculated per supercell and as a function of the control parameter ε for strained P-graphene. S_e and C_e include results for three temperatures, 1, 10, and 100 K, where we have amplified each quantity by 100, 10, and 1, respectively, to superimpose the data. Violet zone for each plot in the range 0% $\leq \varepsilon <$ 5.5%, corresponding to the magnetic phase, and green region 5% $< \varepsilon \leq$ 10% in the nonmagnetic phase. Shading gray rectangles delimit the critical transition region (5% $\leq \varepsilon \leq$ 5.5%).

configuration at absolute zero (T = 0 K), as well as influencing thermodynamic quantities such as the electronic entropy S_e, and electronic specific heat C_e at finite temperatures $T \neq 0$.

At T = 0 K, the system undergoes a MQPT driven by ε, shifting from a magnetic state characterized by an sp^3-type hybridization (0% $\leq \varepsilon \leq$ 5%) to a nonmagnetic state with sp^2 hybridization (5.5% $\leq \varepsilon \leq$ 10%) where the phosphorus atom becomes coplanar with the graphene sheet. At non-zero temperatures, the behavior for S_e and C_e when as a function of ε captures an extension of the MQPT, which presents a distinctive Λ-lineshape response that persists for temperatures around 100 K.

The quantities S_e and C_e are particularly effective in distinguishing between the magnetic and nonmagnetic regimes at finite temperatures, corresponding to the same strain values where the MQPT is observed at T = 0. The transition between these two regimes defines a critical strain region, approximately in the range 5% $\leq \varepsilon \leq$ 5.5%, where a competition between quantum and thermal fluctuations emerges. The Λ-type line shape identified here is crucial for understanding the accessible states near the Fermi level. This behavior could be experimentally probed *via* the thermodynamic responses of S_e and C_e, providing insights into the on–off magnetism occurring at temperatures above zero in strained P-doped graphene.

Author contributions

N. C. and L. M.-M. started the discussions and first ideas. J. H.-T. made the DFT calculations. P. V. made the thermodynamic calculations. N. C. wrote the first version of the manuscript. N. C. and P. V. contributed to the core discussions and wrote the final version of the manuscript. All the authors participated and contributed to the analysis and discussions of the work and reviewed the manuscript.

Data availability

The authors confirm that the data supporting the findings of this study are available within the article.

Conflicts of interest

There are no conflicts to declare.

Acknowledgements

N. C. acknowledges support from ANID Iniciación en Investigación Fondecyt Grant No. 11221088 and DGII-UTA, and the hospitality of Universidad Federico Santa María, Valparaíso, Chile. J. H.-T. acknowledges a postdoctoral fellowship from CONAHCyT-México. The authors thankfully acknowledge the computer resources, technical expertise, and support provided by the Laboratorio Nacional de Supercómputo del Sureste de México (LNS), a member of the CONACYT national laboratories, with project no. 202303063N. One of the authors (R. de Coss) is grateful for the hospitality of the Mesoamerican Centre for Theoretical Physics (MCTP), where part of this work was developed during a research visit. P. V. wishes to thank the Fondecyt grant project No. 1240582.

References

1 R. K. Pathria and P. D. Beale, Phase Transitions: Criticality, Universality And Scaling, in *Statistical Mechanics*, ed. R. K. Pathria and P. D. Beale, Academic Press, 4th edn, 2022, ch. 12, pp. 417–476, https://www.sciencedirect.com/science/article/pii/B978075062469550013X.

2 S. Sachdev, Quantum phase transitions, *Phys. World*, 1999, **12**(4), 33.

3 M. Klanjšek, A critical test of quantum criticality, *Physics*, 2014, **7**, 74.

4 P. Vancsó, I. Hagymási and L. Tapasztó, A magnetic phase-transition graphene transistor with tunable spin polarization, *2D Mater.*, 2017, **4**(2), 024008.

5 D. E. Parker, T. Soejima, J. Hauschild, M. P. Zaletel and N. Bultinck, Strain-induced quantum phase transitions in magic-angle graphene, *Phys. Rev. Lett.*, 2021, **127**(2), 027601.

6 L. Palma-Chilla, J. A. Lazzús and J. Flores, Entropy and Negative Specific Heat of Doped Graphene: Topological Phase Transitions and Nernst's Theorem Revisited, *Entropy*, 2024, **26**(9), 771.

7 A. Huang, S. Ke, J. H. Guan, J. Li and W. K. Lou, Strain-induced topological phase transition in graphene nanoribbons, *Phys. Rev. B*, 2024, **109**(4), 045408.

8 O. V. Yazyev and L. Helm, Defect-induced magnetism in graphene, *Phys. Rev. B: Condens. Matter Mater. Phys.*, 2007, **75**(12), 125408.

9 G. Z. Magda, X. Jin, I. Hagymási, P. Vancsó, Z. Osváth and P. Nemes-Incze, *et al.*, Room-temperature magnetic order on zigzag edges of narrow graphene nanoribbons, *Nature*, 2014, **514**(7524), 608–611.

10 J. Hernández-Tecorralco, L. Meza-Montes, M. Cifuentes-Quintal and R. de Coss, Understanding the sp magnetism in substitutional doped graphene, *Phys. Rev. B: Condens. Matter Mater. Phys.*, 2022, **105**(22), 224425.

11 L. Lin, L. Fu, K. Zhang, J. Chen, W. Zhang and S. Tang, *et al.*, P-superdoped graphene: Synthesis and magnetic properties, *ACS Appl. Mater. Interfaces*, 2019, **11**(42), 39062–39067.

12 R. Langer, P. Błoński, C. Hofer, P. Lazar, K. Mustonen and J. C. Meyer, *et al.*, Tailoring electronic and magnetic properties of graphene by phosphorus doping, *ACS Appl. Mater. Interfaces*, 2020, **12**(30), 34074–34085.

13 C. Lee, X. Wei, J. W. Kysar and J. Hone, Measurement of the elastic properties and intrinsic strength of monolayer graphene, *Science*, 2008, **321**(5887), 385–388.

14 V. M. Pereira, A. Castro Neto and N. Peres, Tight-binding approach to uniaxial strain in graphene, *Phys. Rev. B: Condens. Matter Mater. Phys.*, 2009, **80**(4), 045401.

15 I. Alcón, R. Santiago, J. Ribas-Arino, M. Deumal, I. D. P. Moreira and S. T. Bromley, Controlling pairing of π-conjugated electrons in 2D covalent organic radical frameworks via in-plane strain, *Nat. Commun.*, 2021, **12**(1), 1705.

16 C. Si, Z. Sun and F. Liu, Strain engineering of graphene: a review, *Nanoscale*, 2016, **8**(6), 3207–3217.

17 J. Hernández-Tecorralco, L. Meza-Montes, M. Cifuentes-Quintal and R. de Coss, Effects of biaxial strain on the impurity-induced magnetism in P-doped graphene and N-doped silicene: a first principles study, *J. Phys.: Condens. Matter*, 2020, **32**(25), 255801.

18 N. Hartman, C. Olsen, S. Lüscher, M. Samani, S. Fallahi and G. C. Gardner, *et al.*, Direct entropy measurement in a mesoscopic quantum system, *Nat. Phys.*, 2018, **14**(11), 1083–1086.

19 A. Rozen, J. M. Park, U. Zondiner, Y. Cao, D. Rodan-Legrain and T. Taniguchi, *et al.*, Entropic evidence for a Pomeranchuk effect in magic-angle graphene, *Nature*, 2021, **592**(7853), 214–219.

20 Y. Saito, F. Yang, J. Ge, X. Liu, T. Taniguchi and K. Watanabe, *et al.*, Isospin Pomeranchuk effect in twisted bilayer graphene, *Nature*, 2021, **592**(7853), 220–224.

21 H. Mousavi and J. Khodadadi, Electronic heat capacity and conductivity of gapped graphene, *Phys. E*, 2013, **50**, 11–16.

22 K. Yi, D. Kim and K. S. Park, Low-energy electronic states and heat capacities in graphene strips, *Phys. Rev. B: Condens. Matter Mater. Phys.*, 2007, **76**(11), 115410.

23 M. A. Aamir, J. N. Moore, X. Lu, P. Seifert, D. Englund and K. C. Fong, *et al.*, Ultrasensitive calorimetric measurements of the electronic heat capacity of graphene, *Nano Lett.*, 2021, **21**(12), 5330–5337.

24 P. Giannozzi, S. Baroni, N. Bonini, M. Calandra, R. Car and C. Cavazzoni, *et al.*, Quantum espresso: a modular and open-source software project for quantum simulations of materials, *J. Phys.: Condens. Matter*, 2009, **21**(39), 395502.

25 P. Giannozzi, O. Andreussi, T. Brumme, O. Bunau, M. B. Nardelli and M. Calandra, *et al.*, Advanced capabilities for materials modelling with Quantum Espresso, *J. Phys.: Condens. Matter*, 2017, **29**(46), 465901.

26 A. Dal Corso, Pseudopotentials periodic table: From H to Pu, *Comput. Mater. Sci.*, 2014, **95**, 337–350.

27 J. P. Perdew, K. Burke and M. Ernzerhof, Generalized gradient approximation made simple, *Phys. Rev. Lett.*, 1996, **77**(18), 3865.

28 H. J. Monkhorst and J. D. Pack, Special points for Brillouin-zone integrations, *Phys. Rev. B: Solid State*, 1976, **13**(12), 5188.

29 M. Methfessel and A. Paxton, High-precision sampling for Brillouin-zone integration in metals, *Phys. Rev. B: Condens. Matter Mater. Phys.*, 1989, **40**(6), 3616.

30 Note that the ground state occurs at $\varepsilon = 0\%$ with $M_S = 1\mu_B$ per supercell.

31 N. Cortés, O. Negrete, F. J. Peña and P. Vargas, Gate-tunable charge carrier electrocaloric effect in trilayer graphene, *Sci. Rep.*, 2021, **11**(1), 1–13.

32 N. Cortés, F. J. Peña, O. Negrete and P. Vargas, Proximity-induced spin-polarized magnetocaloric effect in transition metal dichalcogenides, *Phys. Rev. B*, 2022, **105**(1), 014443.

33 Since entropy and specific heat are extensive properties, they can be easily normalized using appropriate factors, such as per atom or in J $(\text{mol K})^{-1}$. In this study, we present the entropy and specific heat values on a per-unit-cell basis, reported in units of eV K^{-1}.

34 Interestingly, the specific heat as a function of T for a superconducting phase transition[35] is similar to the line shape we find here for *S*e and *C*e.

35 R. Szczesniak, A. P. Durajski and M. W. Jarosik, Specific heat and thermodynamic critical field for calcium under the pressure at 120 GPa, *Mod. Phys. Lett. B*, 2012, **26**(08), 1250050.